Technical Article

Research on Particle Assemblage Damper

TOYOUCHI Atsushi

Abstract

Dampers are devices which suppress vibrations that cause harm to vehicles, buildings, and the like. There are various types of dampers, depending upon the application. However, each type of damper comes with its own problems. Typical examples of such problems are that in the case of oil dampers, liquid leakage may occur, and the damping force may be dependent on temperature. Particle dampers suppress vibrations by generating resistance force through the use of particles in place of oil or the like. These dampers can be exemplified as a possible solution to the abovementioned problems. In this study, an investigation and examination were carried out in order to clarify the generative force characteristics and force generation factors of a separated dual chamber single rod-type particle damper which employs a particulate elastomer*. This type of damper holds the possibility of solving these problems by means of a simple structure.

With regard to the damper used in this study, a particle chamber within the cylinder was divided in two by a piston. It was found that when one chamber of the damper was filled with particles, the generative force had the characteristic of being gradually hardening with hysteresis, with great influence exerted by elastic force in the normal direction and frictional force in the tangential direction. The elastic force in this case was mainly accounted for by repulsion force under compression generated by the compression of the particles, and the frictional force was generated by sliding friction between the cylinder and the particles. Furthermore, it was found that in particular, the packing fraction and Young's modulus, which affects the material, exerted a large effect on the maximum generative force and the hysteresis.

When both chambers were filled with particles, contrary to the findings of single-chamber filling, it was found that the frictional force was generated by the sliding friction between the cylinder and rod and the particles, whereby, due to the friction of the rod, a waveform of the generative force was asymmetrical with respect to the origin.

These results were demonstrated by means of simulations of generative force and particle behavior using the distinct element method, as well as by experiments. The simulation results and the experimental results were in good agreement with one another both qualitatively and quantitatively, and it was confirmed that the simulations were able to reliably reproduce the phenomena which occurred in the experiments.

*"Elastomer" is a generic term for a polymer having elasticity. Rubber and the like correspond to this term.

1 Introduction

The particle assemblage damper is a damper filled with small steel or elastomer balls in place of a fluid such as oil as in oil dampers. These spherical particles that fill the damper are fluidized by the movement of a piston to yield a resistive force. [1, 2] The existing oil damper involves problems including liquid leakage and temperature-dependent damping force. One of the possible solutions to the problems is the use of particle dampers. A particle damper using particles of a larger size than the clearance of the sliding part of the damper is free from leakage. For a particle damper using small elastomer balls (hereinafter "elastomer particles"), using elastomer material with excellent heat/cold resistance whose glass transition temperature is low can reduce the temperature dependence of the generative force.

This study used a separated dual chamber single rod-type particle damper which had two chambers divided by a piston and employed elastomer particles. An investigation was carried out to clarify the generative force characteristics and force generation factors or mechanism for two different cases: with particles filling only one of the two chambers and with particles filling both chambers. Elastomer particles were selected with an aim at delivering a high generative force by densely filling them, which was possible thanks to their high elastic deformation. The investigation used two approaches: one is to develop a damping theory based on the distinct element method and the other to simulate generative force and particle behavior. The simulation results were compared with those obtained from experiments using an actual machine to determine the generative force characteristics and mechanism and to verify the adequacy of the developed theory.

Please note that this damper generates a combined elastic and viscous force, although the term "damper" might cause you to imagine a damper that can suppress vibration by exerting a damping force attributable to a pressure loss or viscous resistance of the fluid used. That's why the force generated by this damper is called a "generative force", not a damping force, for clarification purposes.

2 Generative Force Characteristics of Particle Damper with One of the Chambers Filled

2.1 Damper Structure

Fig. 1 shows the general structure of the damper used in simulations and experiments. The internal void of the damper is divided into two chambers by a piston and only the chamber without the rod is filled with spherical particles. The clearance between the piston perimeter and the cylinder bore is very small so that no particles can move freely between the chambers. Friction in the sliding part is negligible as it is considerably smaller than the generative force of the damper. The piston displacement of this damper described in the following sections refers to the movement of the piston in the direction of the z-axis shown in Fig. 1.

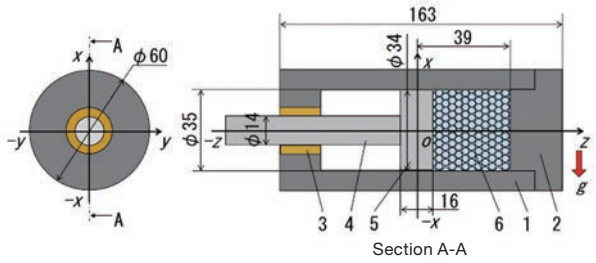

Fig. 1 Damper structure
1. Cylinder, 2. End cover, 3. Bearing, 4. Rod, 5. Piston, 6. Elastomer particles, Unit: mm

2.2 Simulations and Experiments

2.2.1 Distinct Element Method

Simulations were conducted by using the distinct element method (hereinafter "DEM") to clarify the particle behavior, generative force characteristics, and components of the force. DEM is a method for computing the behavior of particles by sequentially calculating the equation of the motion of particles for their translational motion and rotation at individual time points, with consideration given to contact interactions of particles.

2.2.2 Primitive Equation

DEM can be used to determine the velocity and position of a particle by solving the equation of motion expressed in Equation (1) and the equation of angular motion expressed in Equation (2) by taking into account the contact force of each particle.

$$m_i \frac{d^2 \boldsymbol{r}_i}{dt^2} = \boldsymbol{F}_i \tag{1}$$

$$I_i \frac{d\boldsymbol{\Omega}_i}{dt} = \boldsymbol{T}_i \tag{2}$$

where:
i is particle number;
t is time;
m_i is particle mass;
$\boldsymbol{r}_i$ is position vector of the particle;
$\boldsymbol{F}_i$ is the sum total of contact forces;
I_i is inertia moment;
$\boldsymbol{\Omega}_i$ is angular velocity vector of the particle, and;
$\boldsymbol{T}_i$ is the sum total of torques applied to the particle.

$\boldsymbol{F}_i$, $\boldsymbol{T}_i$ and I_i can be expressed in Equations (3) to (5) below:

$$\boldsymbol{F}_i = \boldsymbol{F}_{cn} + \boldsymbol{F}_{ct} + m_i \boldsymbol{g} \tag{3}$$

$$\boldsymbol{T}_i = \boldsymbol{r}_i \times \boldsymbol{F}_{ct} \tag{4}$$

$$I_i = \frac{8}{15} \rho \pi r^5 \tag{5}$$

In the equations above, the subscript n indicates the normal direction at the point of contact and the subscript t the tangential direction at the point of contact. $\boldsymbol{F}_{cn}$ and $\boldsymbol{F}_{ct}$ are the contact force in the normal and tangential directions, respectively. m_i is particle mass, g is gravitational acceleration, p is particle density, and r is particle radius. The concept of contact force was proposed by Cundall and Strack [3]. They used an analysis model consisting of three elements shown in Fig. 2: a spring, a dashpot and a friction slider. The model can be expressed in Equations (6) and (7). Fig. 3 shows a conceptual rendering of the force applied in the normal direction and the force applied in the tangential direction.

$$\boldsymbol{F}_{cn} = \left(-K_n \delta_n^{1.5} - C_n \boldsymbol{V}_{ij} \cdot \boldsymbol{n}_i \right) \boldsymbol{n}_i \tag{6}$$

$$\boldsymbol{F}_{ct} = -K_t \boldsymbol{\delta}_t - C_t \boldsymbol{V}_{fij} \tag{7}$$

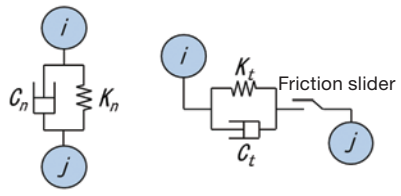

Fig. 2 Contact model
(a) Normal direction, (b) Tangential direction

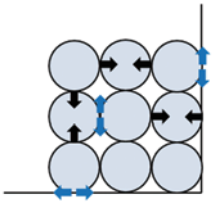

Fig. 3 Conceptual rendering of forces in the normal and tangential directions

In the equations above, K_n and K_t indicate elastic modulus in the normal and tangential directions, respectively, and C_n and C_t are viscosity coefficients in the normal and tangential directions, respectively. δ_n is displacement in the normal direction at the point of contact and $\boldsymbol{\delta}_t$ displacement vector in the tangential direction at the point of contact between the particles i and j. $\boldsymbol{n}_i$ is the unit vector in the normal direction from the particle i to the particle j at their contact point. $\boldsymbol{V}_{ij}$ is the relative velocity vector of the particle i against the particle j. $\boldsymbol{v}_i$ and $\boldsymbol{v}_j$ are velocity vectors of the particles i and j, respectively. $\boldsymbol{V}_{fij}$ is the relative velocity vector in the tangential direction of the particle i against the particle j at their contact point. $\boldsymbol{V}_{ij}$, $\boldsymbol{V}_{fij}$ and $\boldsymbol{\delta}_t$ can be expressed in Equations (8) to (10):

$$\boldsymbol{V}_{ij}=\boldsymbol{v}_i-\boldsymbol{v}_j \tag{8}$$

$$\boldsymbol{V}_{fij}=\boldsymbol{V}_{ij}-(\boldsymbol{V}_{ij}\cdot\boldsymbol{n}_i)\boldsymbol{n}_i+2a(\boldsymbol{\omega}_i-\boldsymbol{\omega}_j)\times\boldsymbol{n}_i \tag{9}$$

$$\boldsymbol{\delta}_t=\Delta t-\boldsymbol{V}_{fij} \tag{10}$$

In the equations above, a is the particle radius, and $\boldsymbol{\omega}_i$ and $\boldsymbol{\omega}_j$ are angular velocity vectors of the particles i and j. Elastic modulus in the tangential direction can be expressed in Equations (11) to (14) using the Hertzian contact theory:

$$K_{nij}=\frac{4}{3\pi}\left(\frac{1}{2\delta_i}\right)\sqrt{\frac{a\delta_n}{2}} \tag{11}$$

$$K_{niw}=\frac{4}{3\pi}\left(\frac{1}{\delta_i+\delta_w}\right)\sqrt{a\delta_n} \tag{12}$$

$$\delta_i=\frac{1-\nu_i^2}{E_i\pi} \tag{13}$$

$$\delta_w=\frac{1-\nu_w^2}{E_w\pi} \tag{14}$$

In the equations above, the subscript w indicates that the relevant amount is related to the wall surface of the cylinder bore (hereinafter "the cylinder wall"). K_{nij} indicates the elastic modulus K_n of the particles during their contact. K_{niw} indicates the elastic modulus K_n of the particle when it makes contact with the cylinder wall. E_i and E_w are the modulus of longitudinal elasticity of the particle and the wall, respectively. ν_i and ν_w are Poisson ratios of the particle and the wall, respectively. The elastic modulus in the tangential direction is based on an assumption that no slide occurs at the point of contact and can be expressed in Equations (15) and (16) in accordance with the Mindlin [4] theory:

$$K_{tij}=\frac{2\sqrt{2a}\,G_i}{2-\nu_i}\delta_n^{0.5} \tag{15}$$

$$K_{tiw}=\frac{8\sqrt{a}\,G_i}{2-\nu_j}\delta_n^{0.5} \tag{16}$$

In the equations above, K_{tij} is the elastic modulus of the particles during their contact. K_{tiw} is the elastic modulus of the particle and the wall during their contact. G_i is the modulus of transverse elasticity of the particle and can be expressed in Equation (17):

$$G_i=\frac{E_i}{2(1+\nu_i)} \tag{17}$$

C_n and C_t can be expressed in Equations (18) and (19):

$$C_n=\alpha\sqrt{m_iK_n}\,\delta_n^{0.25} \tag{18}$$

$$C_t=\alpha\sqrt{m_iK_t}\,\delta_{ct}^{0.25} \tag{19}$$

$$\alpha=2.2\sqrt{\frac{\ln(e)^2}{\ln(e)^2+\pi}} \tag{20}$$

α is a dimensionless constant that decides the magnitude of viscous force and can be expressed in Equation (20). e in Equation (20) is the repulsion coefficient of the particle. If the relative velocity vector in the tangential direction of the particle on the contact surface is more than zero (0) or the contact force in the tangential direction is higher than the frictional force, it is considered that particle sliding has occurred along the contact surface. The phenomenon can be expressed in Equations (21) to (23):

If $|\boldsymbol{V}_{fij}|=0$ and $\boldsymbol{F}_{ct}\leqq\mu_f|\boldsymbol{F}_{cn}|$,

$$\boldsymbol{F}_{ct}=\boldsymbol{F}_{ct} \tag{21}$$

If $\boldsymbol{F}_{ct} > \mu_f \mid \boldsymbol{F}_{cn} \mid$,

$$\boldsymbol{F}_{ct} = -\mu f \mid \boldsymbol{F}_{cn} \mid \boldsymbol{t}_i \tag{22}$$

If $|\boldsymbol{V}_{fij}| > 0$,

$$\boldsymbol{F}_{ct} = -\mu f \mid \boldsymbol{F}_{cn} \mid \boldsymbol{t}_i \tag{23}$$

$$t_i = \frac{\boldsymbol{V}_{fij}}{|\boldsymbol{V}_{fij}|} \tag{24}$$

$\boldsymbol{t}_i$ is unit vector in the $\boldsymbol{V}_{fij}$ direction of the particle and can be expressed in Equation (24). μ_f is the friction coefficient of the particle.

Thus, the analysis model was designed to consider elastic and viscous forces in the normal direction and, in addition to these forces, frictional force as well in the tangential direction. This analysis also applied the second-order accurate Adams-Bashforth method to time-stepping of displacement, velocity and angular velocity.

2.2.3 Simulation and Experimental Conditions

The overview of the experiment equipment is shown in Fig. 4. The simulation conditions are shown in Table 1 and the experimental conditions are shown in Table 2. The particles used in the experiments are shown in Photo 1.

Table 1 Simulation conditions

Particle material	Silicone rubber (TSE 3466 made by Momentive Performance Materials), nitrile rubber (NBR made by Inaba Rubber)
Particle size [mm]	3, 5
Packing fraction [-]	0.60, 0.70
Number of particles	1,339, 1,562
Stroke [mm]	10
Excitation frequency [Hz]	1, 5
Time increments [sec.]	5.0×10^{-9}
Excitation waveform	Sinusoidal
Particle density [kg/m^3]	1.10×10^3
Poisson ratio of particle ν_i	0.5
Friction coefficient μ_f (wall-particle)	0.5
Friction coefficient μ_f (between particles)	0.5
Young's modulus E_w [GPa] (wall)	210
Young's modulus E_i [MPa] (particle)	4.08 (TSE3466), 17.6 (NBR)
Viscosity coefficient α	0.5311

Table 2 Experimental conditions

Particle material	Silicone rubber (TSE 3466), nitrile rubber (NBR)
Young's modulus E_i [MPa] (particle)	4.08(TSE3466), 17.6(NBR)
Particle size [mm]	3, 5
Packing fraction [-]	0.60, 0.70
Stroke [mm]	10
Excitation frequency [Hz]	1, 5

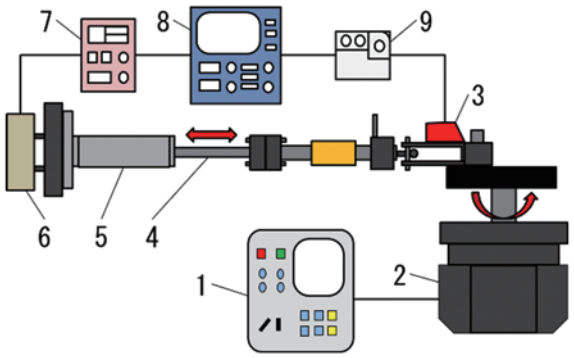

Fig. 4 Experiment equipment
1. Controller, 2. Motor, 3. Laser displacement gauge, 4. Rod, 5. Damper, 6. Load cell, 7. Dynamic distortion amplifier. 8, Oscilloscope, 9. Displacement gauge amplifier unit

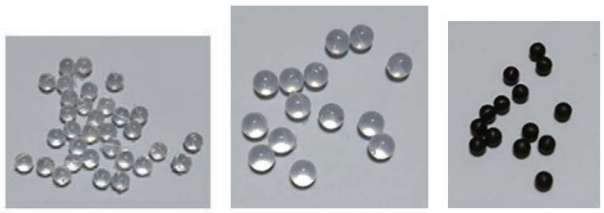

(a) (b) (c)

Photo 1 Particles used
(a) Silicone rubber, particle size 3 mm
(b) Silicone rubber, particle size 5 mm
(c) NBR, particle size 3 mm

For simulation purposes, the general coefficient of friction between rubbers of 0.5 was used as shown in Table 1.[5] In a condition for which two or more parameters are indicated in Table 1 or 2, the one in red is the reference conditions. The packing fraction refers to the ratio of particles in the particle chamber and has been determined by dividing the volume of all the particles present in the chamber by the volume of the chamber.

2.2.4 How to Calculate Generative Force

In the simulations of the particle damper with only one of the chambers filled, the total generative force can be determined, as shown in Fig. 5, by adding the compres-

sive force applied to the cylinder bottom end surface (hereinafter "the cylinder bottom") in the *z*-axis during particle compression by the piston to the frictional force of particles against the cylinder wall in the *z*-axis direction. The component of the generative force in the normal direction is attributable to viscoelasticity of particles due to their compressive deformation. The component of the generative force in the tangential direction is attributable to viscoelasticity of particles due to their shear deformation and sliding friction between particles and the cylinder wall.

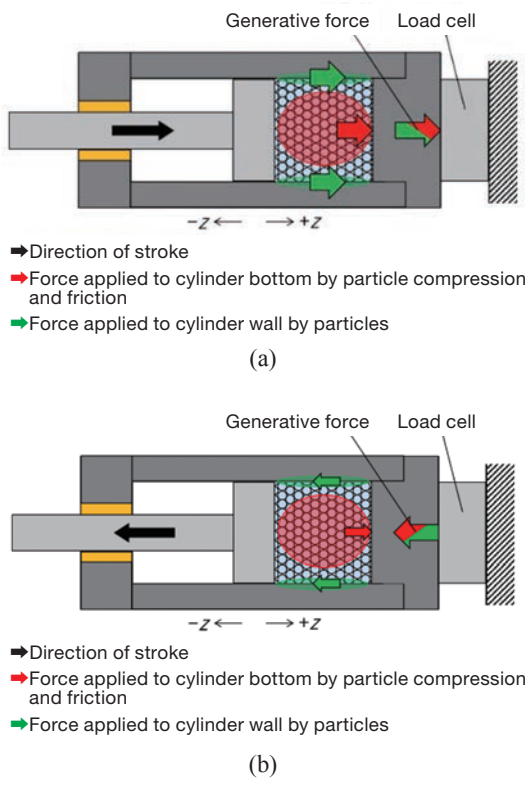

Fig. 5 Generative force in the *z*-axis direction
(a) Positive displacement, (b) Negative displacement

2.2.5 Generative Force and Its Normal and Tangential Components

The results of the simulations are plotted in Fig. 6. These curves show how the generative force and its component in the normal direction (hereinafter "the normal component") and its component in the tangential direction (hereinafter "the tangential component") change with displacement under the reference conditions (i.e., force-displacement curves). Fig. 7 shows the force-velocity curves under the same conditions. All the following figures of these kinds plot a cycle of data. The displacement refers to the piston displacement. The time development of curves is clockwise for force-displacement curves and counterclockwise for force-velocity curves.

According to Fig. 6, the generative force shows gradually hardening characteristics that the generative force increases as the displacement advances in the direction of particle compression (hereinafter "the compression process") and involves hysteresis as the piston travels in the direction opposite to the direction of particle compression (hereinafter "the retraction process"). The gradually hardening characteristics may be attributable to elastic repulsion generated by particle compression. The hysteresis may be attributable to viscosity caused by deformation of elastomer particles and/or friction between particles or between particles and the wall.

Now, let us move on to discussion about the normal and tangential components of the generative force. The normal component is related to resistance generated primarily during particle compression and the tangential component is related to shear force generated between particles or between particles and the wall as well as resistance between particles or between particles and the wall generated when particles move around.

In the compression process, both the normal and tangential components show gradually hardening characteristics as shown in Fig. 6. The normal component has a higher maximum value and lower hysteresis than for the tangential component. Since the normal component peaks at around the point of 0 m/sec. velocity as shown in Fig. 7, the effect of the viscosity attributable to compressive deformation of particles in the normal direction should be trivial, which may result in the gradually hardening characteristics and the lower hysteresis. In other words, the normal component consists predominantly of the elastic force of particles due to their compression. The tangential component also shows gradually hardening characteristics, but has higher hysteresis, resulting in a negative value that gradually becomes smaller as the displacement advances during the retraction process. Since the viscosity affecting the hysteresis depends on the velocity, the effect of viscosity on the tangential component is probably low because it peaks at around 0 m/sec. velocity as shown in Fig. 7. In addition, the force converges to 0 N at a displacement of -5 mm, which is the start point of the compression process. Therefore, the tangential component consists predominantly of frictional force, to which the normal component acts as vertical resistance. As the positive/negative sign to friction force is switched over according to the direction of displacement, the tangential

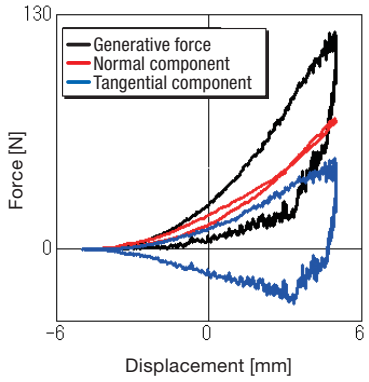

Fig. 6 Force-displacement curves of generative force and its normal and tangential components

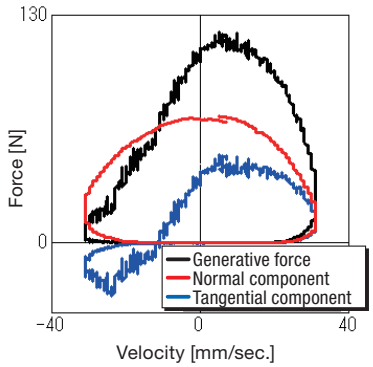

Fig. 7 Force-velocity curves of generative force and its normal and tangential components

component takes a negative value with higher hysteresis during the retraction process. The frictional force generated here refers to the friction of sliding particles against the cylinder wall.

2.2.6 Elastic and Viscous Forces in Normal/ Tangential Direction

To verify the assumption discussed in the previous section that the normal component of the generative force consists predominantly of elastic force and the tangential component consists predominantly of frictional force, this section further discusses these components by dividing them into elastic and viscous forces. Fig. 8 shows the force-displacement curves of the normal component and its breakdown into elastic and viscous forces. Fig. 9 is an enlarged view of the viscosity curve in Fig. 8. Fig. 10 shows the force-displacement curves of the tangential component and its breakdown into elastic and viscous forces.

In Fig. 8, the normal component curve generally agrees with the elasticity curve, which implies that the elastic repulsion of particles due to their compressive deformation is predominant. However, the viscosity never takes a value of zero (0). The enlarged view in Fig. 9 reveals that a minute force is always generated. Fig. 10 shows that the tangential component involves no elastic or viscous force attributable to shear deformation of particles along the cylinder wall. Rather, the tangential component only consists of friction of particles against the cylinder wall, which implies that particles are always sliding along the wall.

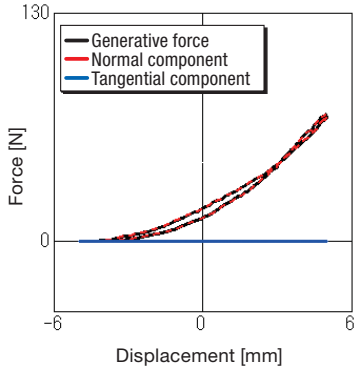

Fig. 8 Force-displacement curves of normal component and its elasticity and viscosity

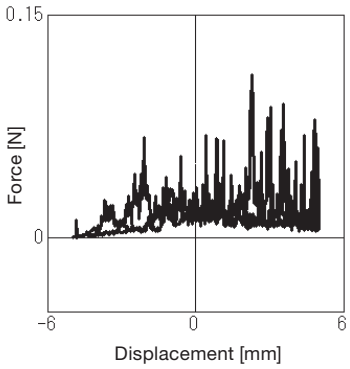

Fig. 9 Enlarged view of force-displacement curve of viscosity of normal component

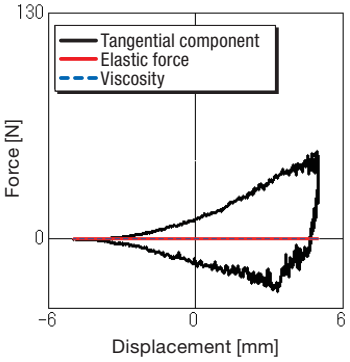

Fig. 10 Force-displacement curves of tangential component and its elasticity and viscosity

Now, the discussion above has revealed that the generative force is greatly affected by the elastic force of particles in the normal direction due to their compressive deformation and the friction of particles against the cylinder wall in the tangential direction.

2.2.7 Distribution of Particle Compression

Since the generative force heavily depends on the elastic force in the normal direction, we tried to determine the effect of the compressive force of particles filled in the damper under the reference conditions. Fig. 11 (a) to (d) show where the piston and particles are located in the damper when viewed from the section A-A in Fig. 1 and the distribution of particle compression. The compressive force on particles in these diagrams is due to the elasticity in the normal direction.

In Fig. 11 (a), many of the particles close to the piston are highly compressed during the compression process, resulting in higher particle repulsion against the piston. Near the cylinder bottom in turn many particles are not so strongly compressed. This means that the compression of the particles close to the piston has not been transferred well to the cylinder bottom. In Fig. 11 (c) for the retraction process, many of the particles close to the piston are not so strongly compressed, resulting in lower particle repulsion against the piston. However, many of the highly com-

pressed particles still remain near the cylinder bottom. This means that the compression of the particles close to the cylinder bottom has not been transferred well to the piston. It can be derived from these facts that there is a time lag between the forced excitation by the piston and the transfer of forces caused by particle deformation.

In the compression process, the particle-particle compressive force, the force pressing particles against the cylinder wall, and the friction against which these two forces act as vertical resistance increase, resulting in a higher force applied to the cylinder bottom. In the retraction process, the particle-particle compressive force and the force pressing particles against the wall become smaller, resulting in lower friction. In this case, the force applied to the cylinder bottom is the sum of the compressive repulsion of particles and the friction. Since the friction is switched from a positive value to a negative one or vice versa between the compression and retraction processes, the generative force at any given displacement during the compression process is different from that at the same displacement during the retraction process. The discussion above has revealed that the delay in the transfer of forces and the friction are one of the causes of the hysteresis of the generative force.

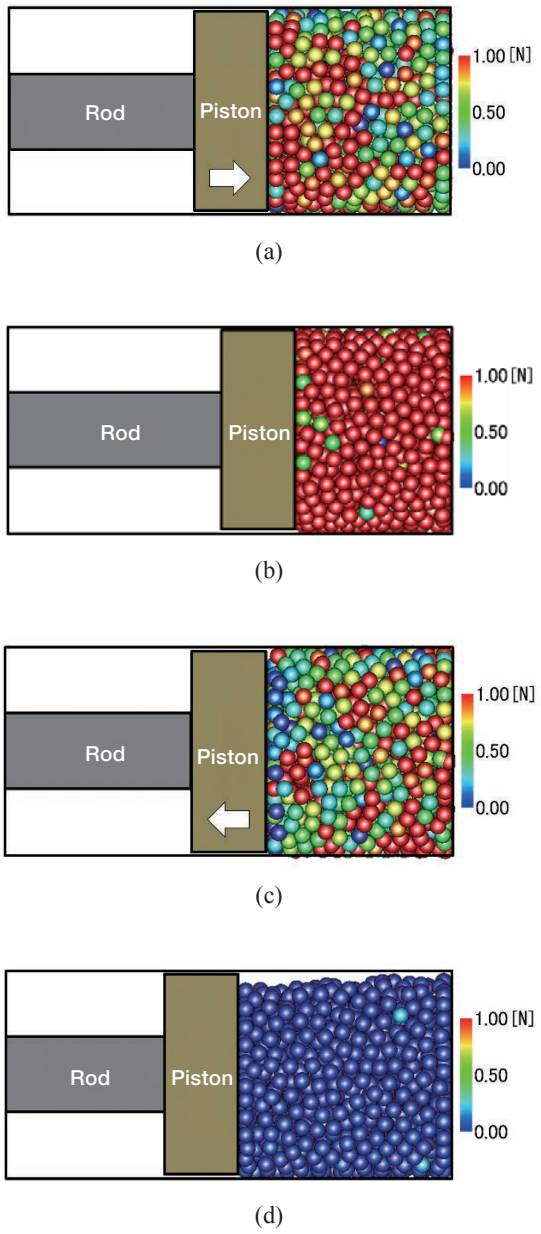

Fig. 11 Distribution of particle compression
(a) Compression process, z = 0
(b) z = 5
(c) Retraction process, z = 0
(d) z = -5

2.2.8 Comparison Between Experimental and Simulation Results

To verify the adequacy of the simulations and determine the generative force characteristics under different conditions, we conducted experiments under different conditions and compared the results with the simulation results. Figs. 12 to 16 show the generative force-displacement curves obtained from the experiments under the reference conditions as well as under another set of conditions where the packing fraction, excitation frequency, particle material and particle size were changed from the reference conditions, along with the results of the simulations. The particle material was changed from the reference conditions in that only the Young's modulus of particles was changed.

According to Figs. 12 to 16, the simulation results are in good agreement with the experimental results both qualitatively and quantitatively. Like under the reference conditions, the generative force shows gradually hardening characteristics during the compression process or hysteresis after the transition from the compression process to the retraction process, regardless of the packing fraction, excitation frequency, particle material or particle size.

Figs. 12 to 16 also show how the generative force changes under different conditions. Its peak and hysteresis substantially change with the packing fraction and the Young's modulus which affects the particle material. They do not change so much with the excitation velocity or

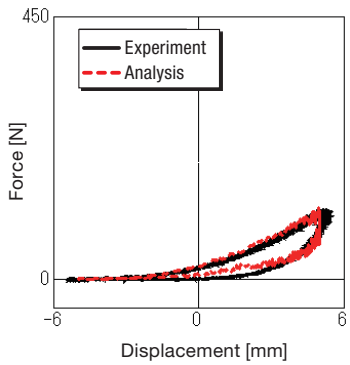

Fig. 12 Generative force-displacement curves; Experiment-simulation comparison
Under reference conditions (packing fraction 0.60, excitation frequency 1 Hz, Young's modulus 4.08 MPa, particle size φ3 mm)

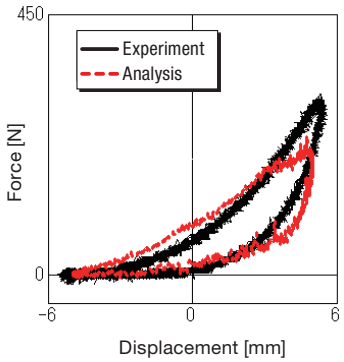

Fig. 13 Generative force-displacement curves; Experiment-simulation comparison
With packing fraction changed (0.70)

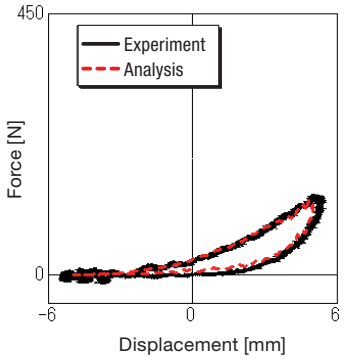

Fig. 14 Generative force-displacement curves; Experiment-simulation comparison
With excitation frequency changed (5 Hz)

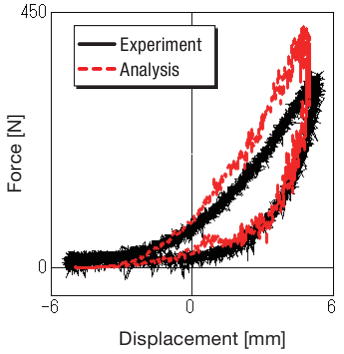

Fig. 15 Generative force-displacement curves; Experiment-simulation comparison
With material changed (Young's modulus 17.6 MPa)

particle size. The reason for the minor effect of excitation velocity is the very small effect of viscosity according to the simulation results. The reason why the particle size does not influence so much is that, if larger particles are used, the particles would have larger deformation as the displacement advances but would have lower friction of particles against the cylinder due to the lower number of particles. This lower friction was a probable cause of why the generative force did not increase so much.

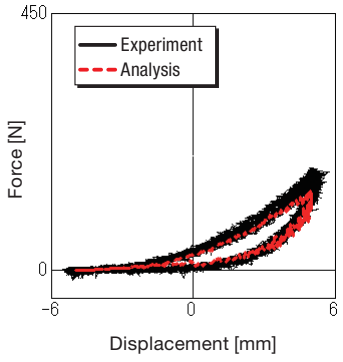

Fig. 16 Generative force-displacement curves; Experiment-simulation comparison
With particle size changed (φ5 mm)

Since the generative force characteristics are found to be qualitatively the same under the different conditions, the particles in the damper should generally behave in a same way. It can now be concluded that the simulations reliably reproduce the phenomena which occurred in the experiments.

3 Characteristics of Generative Force of Particle Damper with Both Chambers Filled

3.1 Damper Structure

Fig. 17 shows the general structure of the damper used for the simulations and experiments. The only difference from the damper described in Chapter 2 is that both chambers divided by the piston are filled with particles. In the case where both chambers are filled with particles, the chamber without the rod is called Chamber A and that with the rod Chamber B.

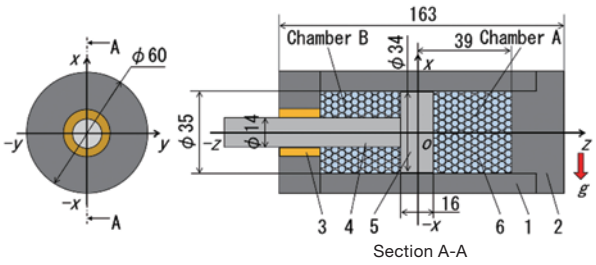

Fig. 17 Damper structure
1. Cylinder, 2. End cover, 3. Bearing, 4. Rod, 5. Piston, 6. Elastomer particles
Unit: mm

3.2 Simulations and Experiments

3.2.1 Simulation and Experimental Conditions

Table 3 shows the simulation conditions. Table 4 shows the experimental conditions. The simulation methods, primitive equations and experimental conditions described in Chapter 2 were also used in these simulations and experiments. The simulations and experiments in this Chapter were conducted only under the reference conditions described in Chapter 2 because the generative force characteristics have been generally verified in Chapter 2.

Table 3 Simulation conditions

Particle material	Silicone rubber (TSE 3466)
Particle size [mm]	3
Packing fraction [-]	0.60
Number of particles	2533
Stroke [mm]	10
Excitation frequency [Hz]	1
Time increments [sec.]	5.0×10^{-9}
Excitation waveform	Sinusoidal
Particle density [kg/m^3]	1.10×10^3
Poisson ratio of particle ν_i	0.5
Friction coefficient μ_f (wall-particles)	0.5
Friction coefficient μ_f (between particles)	0.5
Young's modulus E_w [GPa] (wall)	210
Young's modulus E_i [MPa] (particle)	4.08(TSE3466)
Viscosity coefficient α	0.5311

Table 4 Experimental conditions

Particle material	Silicone rubber (TSE 3466)
Young's modulus E_i [MPa] (particles)	4.08(TSE3466)
Particle size [mm]	3
Packing fraction [-]	0.60
Stroke [mm]	10
Excitation frequency [Hz]	1

3.2.2 How to Calculate Generative Force

In the simulations of the particle damper with both of its chambers filled, the force applied to the cylinder bottom D_z shown in Fig. 18 can be determined by adding the compressive force applied to the cylinder bottom in the z-axis during particle compression by the piston to the frictional force of particles against the cylinder wall in the z-axis direction. For simulations of a damper with both chambers filled with particles, the force applied to the rod end R_z shown in Fig. 19 can be determined by adding the compressive repulsion applied to the rod end in the z-axis during particle compression by the piston to the frictional force of particles against the rod wall in the z-axis direction. There is a balance between D_z and R_z.

The normal component of the generative force is attributable to Viscoelasticity generated by compressive deformation of particles. The tangential component of the

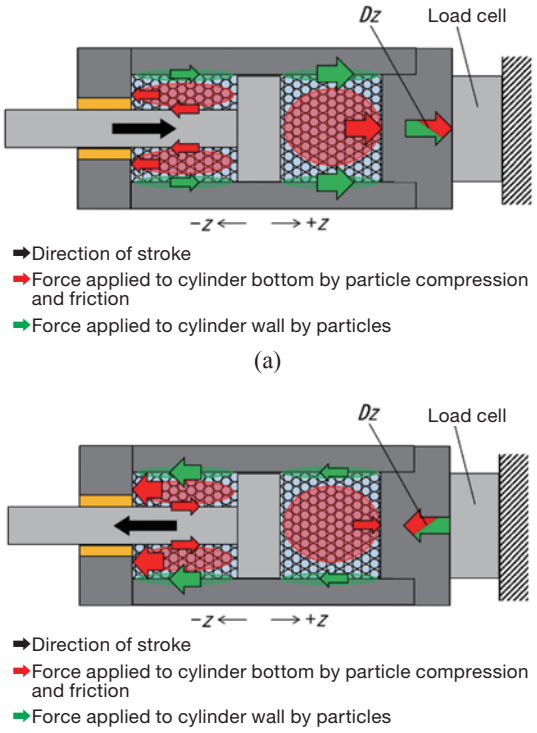

Fig. 18 Force applied to cylinder bottom in the z-axis direction
(a) Positive displacement, (b) Negative displacement

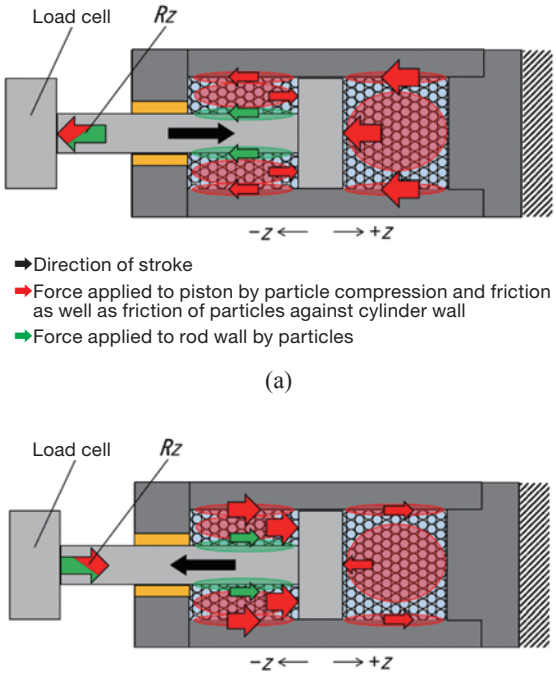

Fig. 19 Force applied to rod end in the z-axis direction
(a) Positive displacement, (b) Negative displacement

generative force is attributable to Viscoelasticity generated by shear deformation of particles and the sliding friction of particles against the cylinder or rod wall. Therefore, determining D_z will identify the friction of particles against the cylinder wall and determining R_z will identify the friction of particles against the rod wall.

3.2.3 Generative Force and its Breakdown

As shown in Fig. 18, simulations were conducted with a focus on the force applied to the cylinder wall. The simulations produced the results shown in Figs. 20 and 21. Fig. 20 shows the generative force D_z that changes with displacement under the reference conditions, the tangential component of D_z applied to the cylinder wall, and the remaining component. Fig. 21 shows the generative force D_z that changes with velocity under the same conditions. The remaining component was determined by subtracting the tangential component applied to the cylinder wall from Dz. According to Fig. 20, the generative force shows hardening characteristics and involves hysteresis after the direction of displacement changes. In general, the maximum generative force during the negative displacement in which the particles in Chamber B are predominantly compressed is larger than the maximum generative force during the positive displacement in which the particles in Chamber A are predominantly compressed. The curve of the generative force is asymmetrical with respect to the origin. Like the damper with one of the chambers filled with particles, this damper also delivers the generative force with gradually hardening characteristics probably because of the effect of the elastic repulsion due to particle compression. The hysteresis is attributable to the viscosity due to deformation of the elastomer particles and/or the effect of the particle-particle or particle-wall friction. The generative force has been plotted to be a nonlinear curve probably because, as the piston moves toward Chamber B where the rod exists to increase the displacement, the particle-rod friction increases.

The next step is to discuss the generative force characteristics based on the force applied to the cylinder wall and the remaining component. Fig. 20 indicates that, as the displacement advances in each direction, both the force applied to the cylinder wall and the remaining component increase. In this process, the force applied to the cylinder wall abruptly jumps when the direction of displacement changes. After a certain point of displacement, the force mildly increases to show gradually hardening characteristics. On the other hand, the remaining component involves this gradually hardening characteristics all the time. So, the hysteresis is considered to be greatly influenced by the force applied to the cylinder wall. The maximum generative force is attributable to the force applied to the cylinder wall and the remaining component to almost the same extent. Here again, as in Fig. 18, the generative force applied to the cylinder bottom on the side without the rod consists of the normal compression generated when the piston compresses particles, the tangential friction of particles against the rod wall, and the tangential friction of particles against the cylinder wall. The asymmetry of the generative force curve to the origin is attributable to the contact force of particles against the rod located in Chamber B. This issue will be verified later in the section discussing the results related to the generative force R_z.

Fig. 21 shows that the generative force and its normal and tangential components' peak at a point slightly shifted from the 0 m/sec. velocity. Without the influence of viscosity, the force-displacement curve should peak at the point of 0 m/sec. velocity. According to Equations (6) and (7), the velocity only affects the normal/tangential viscosity. Therefore, the maximum generative force occurs at a point slightly shifted from 0 m/sec. probably because of the effect of viscosity.

Then, another simulation was conducted with a focus on the force applied to the rod wall as shown in Fig. 19.

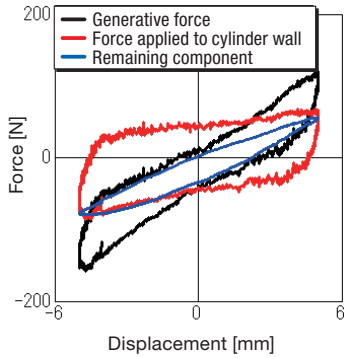

Fig. 20 Force-displacement curves of generative force D_z, force applied to cylinder wall and remaining component

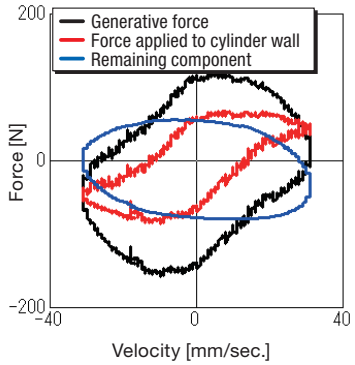

Fig. 21 Force-velocity curves of generative force D_z, force applied to cylinder wall, and remaining component

Fig. 22 shows the generative force R_z that changes with displacement under the reference conditions, its tangential component applied to the rod wall, and the remaining component. The remaining component was determined by subtracting the tangential component of the force applied to rod wall from R_z. The only difference from D_z is that the force applied to the rod wall shows gradually hardening

characteristics during the negative displacement, and increases until the displacement increases to a certain positive level and then gradually decreases until it gets down to about 0 N. The remaining component shows almost the same characteristics as those of the generative force however considerably differs from the generative force in the negative displacement region. The force applied to the rod wall shows gradually hardening characteristics as the friction of particles against the rod wall, which acts as vertical resistance, increases due to the increase in particle compression in Chamber B caused by negative displacement. During the positive displacement, the friction of particles against the rod wall decreases because the particle compression in Chamber B decreases. Furthermore, this force applied to the rod wall makes the generative force asymmetrical with respect to the origin. The gradually hardening characteristics of the remaining component is attributable to the compressive repulsion of particles and the friction of particles against the cylinder wall, which acts as vertical resistance. The hysteresis is attributable to the friction of particles against the cylinder wall.

Now the force applied to the cylinder wall shown in Fig. 20 can be compared with the force applied to the rod wall shown in Fig. 22. It is obvious that the force applied to the rod wall is smaller. This is because the rod has a smaller outside diameter than the cylinder bore. In other words, since the rod perimeter has a smaller surface area, the rod is affected by particle friction to a smaller degree than the cylinder is affected by the same.

From the above, the discussion about D_z and R_z can be summarized as follows. The generative force in Chamber A mainly consists of the normal repulsion generated during particle compression by the piston and the tangential friction of particles against the cylinder. In Chamber B, the tangential friction of particles against the rod is added to the forces stated above to constitute the generative force. Furthermore, the generative force, the force applied to the cylinder wall, and the remaining component peak at a point shifted from the 0 m/sec. velocity as shown in Fig. 21. This implies that these forces are affected by the viscous force of elastomer particles.

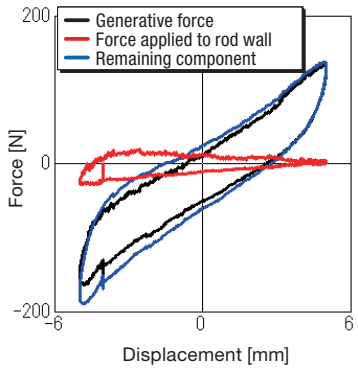

Fig. 22 Force-displacement curves of generative force R_z, force applied to rod wall, and remaining component

3.2.4 Elasticity and Viscosity of Force Applied to Cylinder or Rod Wall and of Remaining Component of Generative Force

To verify the effect of viscosity described in the previous section, the force applied to the cylinder or rod wall and the remaining component of the generative force were divided into elasticity and viscosity.

Fig. 23 shows the force-displacement curves of the force of D_z applied to the cylinder wall and its elasticity and viscosity. Fig. 24 shows the force-displacement curves of the remaining component of D_z and its elasticity and viscosity. Fig. 25 is an enlarged view of Fig. 24 showing the viscosity.

According to Fig. 23, the force applied to the cylinder wall only consists of the friction of particles against the cylinder. No elastic or viscous force is generated due to shear deformation of particles. Like the discussion about the tangential component of the generative force in the particle damper with one of the chambers filled, this damper also has sliding of particles against the cylinder in the tangential direction all the time. According to Fig. 24, the remaining component consists predominantly of elasticity with gradually hardening characteristics and hysteresis. The remaining component is generally in good agreement with the elasticity. Therefore, like the normal component of the particle damper with one of the chambers filled, this damper also delivers the generative force whose remaining component consists predominantly of the elastic repulsion due to compressive deformation of particles. The effect of the viscous force generated during particle deformation is very small. Unlike the normal component of the particle damper with one of the chambers filled, this damper delivers the generative force whose elasticity involves hysteresis. This is because the elastic modulus finally formed by the particle groups filled in chamber A and chamber B are different in each chambers. Another reason is, according to Fig. 18, that the elastic force of this damper includes the frictional force of particles against the rod. Therefore, properly speaking, this is not an elastic force or elasticity, but it is called here an elastic force or elasticity for convenience purposes. The viscous force never takes a value of zero (0). Rather, a minute viscous force is generated as shown in Fig. 25.

Fig. 26 shows the force-displacement curves of the force of R_z applied to the rod wall and its elasticity and viscosity. Fig. 27 shows the remaining component of R_z and its elasticity and viscosity. Fig. 28 shows an enlarged view of the viscosity curve in Fig. 27.

According to Fig. 26, like D_z, R_z also comes with the force applied to the rod wall only consisting of the friction of particles against the rod. No elastic or viscous force is generated by particle deformation. This means that particles around the rod are sliding all the time. According to Fig. 27, like D_z, R_z also comes with the remaining component consisting predominantly of elasticity with gradually hardening characteristics and hysteresis. The remaining

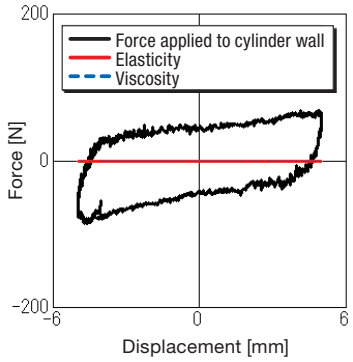

Fig. 23 Force-displacement curves of component of generative force D_z applied to cylinder wall and its elasticity and viscosity

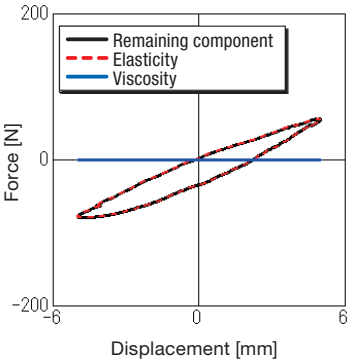

Fig. 24 Force-displacement curves of remaining component of generative force D_z and its elasticity and viscosity

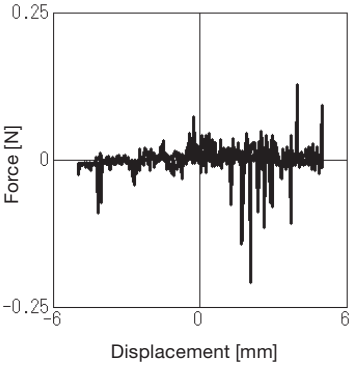

Fig. 25 Enlarged view of force-displacement curve of viscosity of remaining component (in Fig. 24)

component is generally in good agreement with the elasticity. Properly speaking, according to Fig. 19, this is not an elastic force because the elasticity in Fig. 27 consists of the elastic repulsion of particles during compressive deformation and the friction between the cylinder and particles, but it is called here an elastic force or elasticity as in the case of the force applied to the cylinder wall and the remaining component. The reason why the elastic force involves hysteresis is that, like D_z, the chambers show different non-linear Young's modulus values depending on the presence/absence of the rod. Another reason is, according to Fig. 19, that the generative force of this damper includes the friction between the cylinder and particles. Like D_z, R_z also includes a minute viscous force as shown in Fig. 28.

Now it may be useful to compare the generative force characteristics of this elastomer particle damper with the repulsion characteristics of cylindrical or other-shaped elastomer blocks during compression. When elastomer cylinders are compressed, many of them produce the generative force that depends on the displacement and involves viscoelasticity with hysteresis. In this damper in turn, friction of elastomer particles against the cylinder or

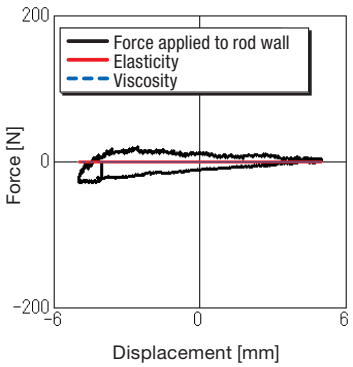

Fig. 26 Force-displacement curves of component of generative force R_z applied to rod wall and its elasticity and viscosity

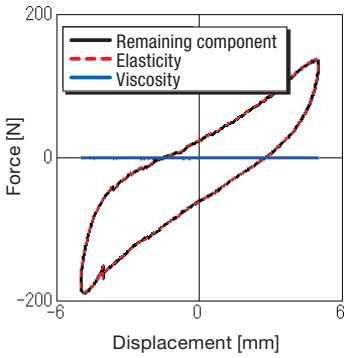

Fig. 27 Force-displacement curves of remaining component of generative force R_z and its elasticity and viscosity

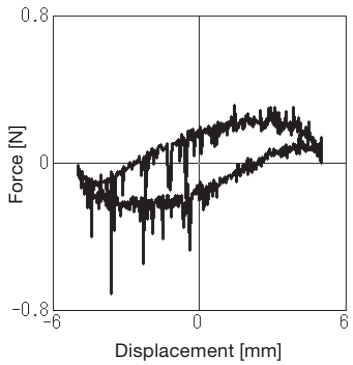

Fig. 28 Enlarged view of force-displacement curve of viscosity of remaining component (in Fig. 27)

rod wall occurs to greatly affect the generative force. Thus, the generative force of this damper shows higher hysteresis in comparison with the characteristics of the elastomer block of the same volume when it is compressed.

3.2.5 Distribution of Particle Compression

Like the particle damper with one of the chambers filled, this damper with both chambers filled also produces the generative force D_z heavily dependent on the other components than that applied to the cylinder wall, that is, particularly the elastic force in the normal direction. Then, we tried to determine the effect of the compressive force applied to particles filled in the damper. Fig. 29 (a) to (d) show where the piston and particles are located in the damper when viewed from section A-A in Fig. 17 and the distribution of particle compression. The compressive force applied to particles in these diagrams is due to the elasticity in the normal direction.

In Fig. 29 (a), as the piston travels in the direction of positive displacement, many of the particles close to the piston in Chamber A are highly compressed while many of the particles close to the cylinder bottom are weakly compressed. In Chamber B, many of the particles close to the piston are weakly compressed while many of the particles close to the cylinder bottom are highly compressed. This means that, as the piston travels in the direction of positive displacement, the force applied to the piston by the particles in the Chamber A increases while the force applied to the piston in Chamber B decreases. This phenomenon also takes place when the piston travels in the opposite direction as shown in Fig. 29 (c). However, a comparison between Figs. 29 (a) and 29 (c) reveals that Chamber B in Fig. 29 (c) has a greater number of highly compressed particles than in Chamber A in Fig. 29 (a) while Chamber A in Fig. 29 (c) has a greater number of weakly compressed particles than in Chamber B in Fig. 29 (a). This means that the compressive force applied to particles in Chamber B during displacement in the negative direction has greater influence. This is probably because Chamber B has a smaller volume than Chamber A by the volume of the rod, thereby giving particles smaller space to escape in Chamber B. As a result, particle compression in Chamber B is started at a smaller displacement than in Chamber A. In addition, a delay in the transfer of the force due to particle deformation can be found in Fig. 29 as in the case of the damper with one of the chambers filled.

3.2.6 Comparison Between Experimental and Simulation Results

To verify the adequacy of the simulations, we conducted experiments and compared the results with the simulation results. Fig. 30 shows the generative force-displacement curves obtained from the experiments and simulations.

According to Fig. 30, the simulation results are in good agreement with the experimental results both qualitatively and quantitatively. It can now be concluded that the simu-

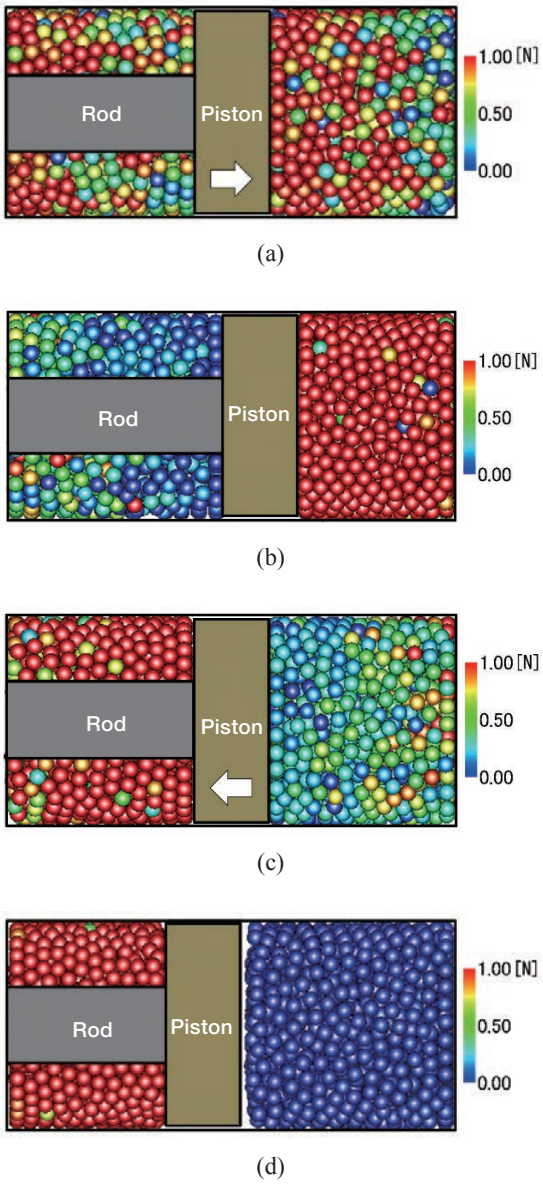

Fig. 29 Distribution of particle compression
(a) Compression process, z = 0
(b) z = 5
(c) Retraction process, z = 0
(d) z = -5

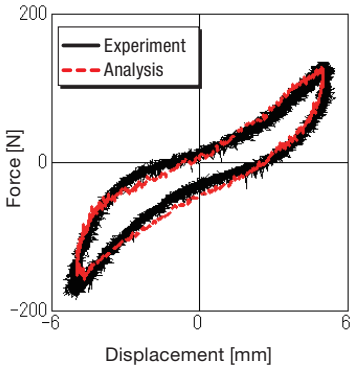

Fig. 30 Generative force-displacement curves; Experiment-simulation comparison

lations reliably reproduce the phenomena which occurred in the experiments, as in the case of the damper with one of the chambers filled.

4 Concluding Remarks

In this study, an investigation and discussions were conducted to clarify the generative force characteristics and force generation factors of a separated dual chamber single rod-type damper using elastomer particles for the two cases of one of the chambers filled and both chambers filled.

When only one of the chambers is filled with particles, the generative force shows gradually hardening characteristics along with hysteresis and is greatly affected by the elasticity in the normal direction and the friction in the tangential direction. This elasticity is mainly attributable to the compressive repulsion of particles during compression. The friction here indicates the sliding friction of particles against the cylinder. Increasing the packing fraction, the excitation frequency, the Young's modulus which affects the particle material, and the particle size will raise the maximum generative force and hysteresis. In particular, the packing fraction and Young's modulus strongly affect the generative force.

With both chambers filled with particles, the generative force shows gradually hardening characteristics along with hysteresis and is affected by the frictional force applied to the cylinder and rod walls in the tangential direction and the elasticity included in the remaining component, as in the case of the damper with one of the chambers filled. The force-displacement curve of the generative force is asymmetrical with respect to the origin because of the frictional force applied to the rod wall.

The results of DEM-based simulations of a damper with one of the chambers filled and a damper with both chambers filled were in good agreement with the experimental results both qualitatively and quantitatively. This has proved that the simulations reliably reproduce the phenomena which occurred in the experiments.

This report has now successfully clarified the generative force characteristics and force generation factors.

A future challenge is to enhance the accuracy of discussions and analyses. This report has mainly discussed the generative force based on its force-displacement curves and distribution of particle compression. Rather, we should determine the variations in elastic modulus of particles and the amount of particle deformation in the analysis process and then verify them in connection with the equations used for analysis. Furthermore, when considering to commercialize the damper, we also need to determine how the generative force changes with the size of the piston or the length of the particle chambers and to clarify advantages and disadvantages of this damper compared with other types of dampers.

Note) This report has been prepared by re-editing the FY2020 doctoral dissertation thesis in Nagoya Institute of Technology: Generative Force Characteristics of Separated Dual Chamber Single Rod-type Particle Damper Using Elastomer Particles.

References

1) IDO Y, HAYASHI K: Damping Force of Damper Utilizing a Spherical Particle Assemblage, Proceedings of 15th International Conference on Experimental Mechanics, 2012, Paper ref: 2714.
2) MORISHITA Y, IDO Y, MAEKAWA K, TOYOUCHI A: Basic Damping Property of a Double Rod Type Damper Utilizing an Elastomer Particle Assemblage, Advanced Experimental Mechanics, Vol. 1, 2016, pp. 93-98.
3) P.A. Cundall, O.D.L. Strack: A Discrete Numerical Model for Granular Assemblies, Géotechnique, Vol. 29, Issue I, 1979, pp. 47-65.
4) R.D. Mindlin: Compliance of Elastic Bodies in Contact, Transaction of ASME, Series E, Journal of Applied Mechanics, Vol. 16, 1949, pp. 259-268.
5) The Japan Society of Mechanical Engineers, JSME Mechanical Engineers' Handbook, Vol. 6, 1977, pp. 3-34, Maruzen Publishing Co., Ltd.

Author

TOYOUCHI Atsushi

Joined the company in 2009
New Products Development Sect.,
Developmental Center, Engineering
Headquarters, Automotive
Components Operations
Engaged in research and
development of particle assemblage
dampers